

# One- and two-photon fluorescence excitation spectra of the $2^1A_g$ states of linear tetraenes in free jet expansions

Hrvoje Petek,<sup>a)</sup> Andrew J. Bell,<sup>b)</sup> Young S. Choi,<sup>c)</sup> and Keitaro Yoshihara  
*Institute for Molecular Science, Myodaiji, Okazaki 444, Japan*

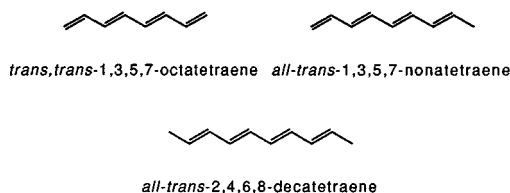
Brett A. Tounge<sup>d)</sup> and Ronald L. Christensen  
*Department of Chemistry, Bowdoin College, Brunswick, Maine 04011*

(Received 19 July 1994; accepted 15 December 1994)

One- and two-photon fluorescence excitation spectra of the  $S_1 \leftarrow S_0$  transitions of the all-*trans* isomers of 1,3,5,7-octatetraene, 1,3,5,7-nonatetraene, and 2,4,6,8-decatetraene have been obtained in free jet expansions. Comparison of the one- and two-photon spectra allows the unambiguous identification of electronic and vibronic origins and, for octatetraene and decatetraene, provides clear evidence for molecular inversion symmetry. One-photon spectra show  $a_g$  progressions built on Herzberg–Teller,  $b_u$  promoting modes, while two-photon spectra are built on progressions of  $a_g$  modes starting from the  $2^1A_g \leftarrow 1^1A_g$  electronic origins. In nonatetraene, the absence of inversion symmetry results in an allowed electronic origin in both the one- and two-photon spectra. Nevertheless, bands built on vibronic origins dominate the one-photon spectrum. The  $S_1 \leftarrow S_0$  spectra of nonatetraene and decatetraene exhibit characteristic splittings of vibronic bands that can be quantitatively explained by the tunneling of the methyl groups through low energy, torsional barriers in the  $S_1$  states. Couplings between methyl torsions and low frequency skeletal modes further complicate the optical spectra. Fluorescence lifetimes indicate abrupt onsets of nonradiative decay processes (tentatively attributed to *trans*→*cis* isomerization) at  $\sim 2100\text{ cm}^{-1}$  excess energy. Systematic differences in the energy dependencies of  $S_1$  nonradiative decays in the three polyenes can be explained by the higher densities of vibronic states in the methyl-substituted compounds. © 1995 American Institute of Physics.

## I. INTRODUCTION

Studying the excited electronic states of simple, linear polyenes in the gas phase is an essential step toward understanding how more complex molecules function in photobiological systems.<sup>1,2</sup> The conversion of light into chemical energy in plants and animals involves carotenoids and retinals.<sup>3–7</sup> Photobiological systems exploit the ability of these polyene chromophores to undergo *cis*–*trans* isomerizations, transfer electrons and protons, or transfer electronic energy, on picosecond or shorter time scales. Advances in time-resolved techniques allow direct measurements of these processes and provide insights into excited state structures and dynamics. However, due to the complexity of the interactions of the chromophores with their environments and the difficulties in modeling such large molecules by high-level calculations, the connections between the photophysical properties of polyene excited states and the photobiological functions of polyene chromophores are still unclear. To better understand the low-lying electronic states of polyenes we have studied *trans,trans*-1,3,5,7-octatetraene, all-*trans*-1,3,5,7-nonatetraene, and all-*trans*-2,4,6,8-decatetraene in free jet expansions,



Detailed studies of these molecules under isolated conditions should lead to a better theoretical understanding of their low-lying electronic states and allow extrapolation to more complex polyene systems.

In 1972 experimental observations by Hudson and Kohler<sup>8</sup> and theoretical calculations by Shulten, Ohmine, and Karplus<sup>9,10</sup> established that the lowest excited state of linear polyenes is a highly correlated  $2^1A_g$  state ( $S_1$ ) rather than the HOMO to LUMO,  $\pi\pi^*$  ( $1^1B_u$ ) state predicted by simple molecular orbital theories. (Following usual practice, we will use  $C_{2h}$  symmetry labels throughout this paper, even for polyenes such as nonatetraene which does not have a rigorous center of symmetry. This convention is justified by the fact that the less symmetrical molecules retain many of the spectroscopic characteristics of polyenes with  $C_{2h}$  symmetry.) The correct energy ordering of the  $2^1A_g$  ( $S_1$ ) and  $1^1B_u$  ( $S_2$ ) states had not previously been understood, in large part because the  $2^1A_g \leftarrow 1^1A_g$  transitions are too weak to observe by standard absorption techniques and because the effects of  $\pi$ -electron correlation had not been sufficiently accounted for in earlier theoretical treatments of linearly conjugated systems.

The radiative and nonradiative decays of the low-lying

<sup>a)</sup>Present address: Advanced Research Laboratory, Hitachi, Ltd., Hatoyama, Saitama, 350-03 Japan.

<sup>b)</sup>Present address: DAD, CBDE, Porton Down, Salisbury, Wiltshire SP4 0JQ United Kingdom.

<sup>c)</sup>Present address: Department of Chemistry, Inha University, Incheon, 402-751 South Korea.

<sup>d)</sup>Present address: Department of Chemistry, Yale University, New Haven, Connecticut 06511.

electronically excited states of polyenes depend on the vibronic interactions between the  $S_2$ ,  $S_1$ , and  $S_0$  states. Herzberg–Teller coupling<sup>11,12</sup> between the  $1^1A_g$  and  $1^1B_u$  states makes  $2^1A_g \leftrightarrow 1^1A_g$  transitions vibronically allowed. One-photon spectra thus are built on vibronic origins due to  $b_u$  promoting modes. Vibronic coupling between  $2^1A_g$  and  $1^1A_g$  states is induced by high-frequency, totally symmetric vibrations.  $S_1 \leftarrow S_0$  excitation results in inversion of carbon–carbon bond orders, leading to a significant reduction in activation energies for *cis*–*trans* isomerizations in the  $S_1$  states.<sup>5,7,13,14</sup> Bond order inversions also induce large Duschinsky rotations<sup>15</sup> and the displacement of normal modes with large CC stretching amplitudes. As a result of  $S_1$ – $S_0$  vibronic coupling, the C=C stretching frequencies are anomalously high in  $S_1$  states and correspondingly low in  $S_0$  states.<sup>12,16,17</sup> The combined effect of the displacements and differences in curvatures for CC stretching coordinates in the  $S_1$  and  $S_0$  states also makes these high frequency vibrations good accepting modes for  $S_1 \rightarrow S_0$  internal conversion.

The role of vibronic coupling on the nonradiative decay of polyene singlet states (decay of the  $S_2$  and  $S_1$  states by intersystem crossing is thought to be insignificant<sup>5</sup>) can be studied as a function of the length of conjugation. For a homologous series of polyenes, the  $S_1$ – $S_0$  energy difference decreases and the  $S_2$ – $S_1$  energy difference increases with increasing conjugation.<sup>5</sup> Another effect of the differences in CC stretching coordinates is that the vertical energies change with conjugation length even more rapidly than the equilibrium energies.<sup>18</sup> In addition, the excited states of shorter polyenes such as dienes and trienes most likely do not have planar geometries. Out-of-plane motions enhance nonradiative decay,<sup>13,14,19</sup> and simple dienes and trienes are essentially nonfluorescent. Fluorescence has been detected for trienes in which large amplitude, out-of-plane motions are restricted by rigid ring structures.<sup>5</sup> *Cis* isomers of hexatriene and octatrienes also emit in cold, supersonic expansions, though these molecules have low fluorescence quantum yields due to competing nonradiative processes with low activation energies.<sup>20</sup>

By contrast, intermediate length polyenes with four to six conjugated double bonds show strong  $S_1 \rightarrow S_0$  fluorescence. Indeed, much of what we know about the  $S_1$  states of polyenes has been obtained from fluorescence excitation and emission spectra of tetraene-doped, *n*-alkane crystals at low temperatures.<sup>5,21</sup> Condensed phase studies of several isomers of octatetraene have shown that solvents can have significant effects on the electronic structure of the  $S_1$  state.<sup>22–25</sup> The  $2^1A_g \leftarrow 1^1A_g$  spectra of all-*trans* isomers either are vibronically allowed or electronically allowed, depending on the symmetry of the electrostatic interactions with the solvent cage.<sup>26</sup> The solvent environment provides a strong perturbation because local electric fields, even within crystals of non-polar solvents, can have gradients of  $10^6$  V/cm.<sup>27,28</sup> When an all-*trans* polyene occupies a lattice site without inversion symmetry, incomplete cancellation of these gradients sufficiently perturbs the polyene to make the  $2^1A_g \leftarrow 1^1A_g$  transition symmetry-allowed. The polarizability of the solvent also reduces the  $S_2$ – $S_1$  energy difference, further increasing

the strength of vibronic coupling. This not only affects the spectra, but also increases the rates of fluorescence decay.

Due to strong perturbations by solvent environments, it is desirable to study polyenes in the gas phase, so that the properties of isolated molecules can be compared directly with theory. This goal has been difficult to reach, due to the instability of simple polyenes (i.e., polyenes with appreciable vapor pressures) and the problems of synthesizing isomerically pure samples in the quantities required for jet experiments. However, several short polyenes are available commercially, and the large  $1^1B_u \leftarrow 1^1A_g$  transition moments and relatively high vapor pressures of butadiene, hexatriene, and octatetraene allowed their  $S_2 \leftarrow S_0$  absorptions to be studied in supersonic molecular beams.<sup>29</sup> Vaida and co-workers suggested that the homogenous broadening of vibronic bands in these spectra was due to  $S_2 \rightarrow S_1$  internal conversion on femtosecond time scales and that the rate of nonradiative decay decreases with the length of conjugation. The fluorescence excitation spectrum of the  $S_2 \leftarrow S_0$  transition of octatetraene also was obtained in a supersonic jet.<sup>30</sup> However, until recently the weak, symmetry-forbidden  $S_1 \leftrightarrow S_0$  transitions of linear polyenes had not been studied in the gas phase, in large part because of earlier reports of vanishingly small  $S_1$  state fluorescence yields under isolated conditions.<sup>5,31–33</sup>

Two developments have opened the study of the  $S_1$  states of polyenes in molecular beams. Kohler and co-workers employed one-color, resonance-enhanced multiphoton ionization (REMPI) techniques to record  $S_1 \leftarrow S_0$  spectra of *cis*-hexatriene,<sup>33</sup> *cis*-isomers of alkyl substituted trienes,<sup>34</sup> 1-phenyl-butadiene, and 1-phenyl-hexatriene.<sup>35</sup> We subsequently obtained the fluorescence excitation spectra of *cis*-hexatriene and a *cis*-isomer of octatriene, demonstrating that under isolated molecule conditions even some simple trienes are weakly fluorescent.<sup>20</sup> Measurements of fluorescence lifetimes and comparison of the fluorescence excitation intensities with those of the corresponding peaks in the REMPI spectrum established that trienes have nonradiative channels with activation energies of  $<200$  cm<sup>-1</sup>, possibly due to *cis*–*trans* isomerization. The intensity of fluorescence excitation spectra of trienes rapidly vanishes beyond this threshold, while the REMPI technique gives structured spectra at much higher vibrational energies.<sup>33,34</sup>

Fluorescence techniques have proven particularly useful for the study of longer polyenes under isolated conditions. Bouwman *et al.* discovered  $S_2 \rightarrow S_0$  and  $S_1 \rightarrow S_0$  emissions of room temperature vapors of tetraenes and pentaenes and obtained the  $S_2 \leftarrow S_0$  fluorescence excitation spectrum of all-*trans*-decatetraene in a supersonic jet.<sup>36</sup> The discovery that intermediate length, gaseous polyenes fluoresce from both their  $S_1$  and  $S_2$  states at room temperature allowed preliminary investigations of the fluorescence excitation and emission spectra of the  $S_2 \leftrightarrow S_0$  and  $S_1 \leftrightarrow S_0$  transitions of tetraenes in supersonic expansions.<sup>36–38</sup> Later, the two-color, resonance-enhanced, two-photon ionization technique (2C-RE2PI; unlike trienes, one-color two-photon ionization cannot be used to measure the  $S_1 \leftarrow S_0$  spectrum of tetraenes) was applied to the  $S_1 \leftarrow S_0$  spectrum of a mixture of octatetraene isomers.<sup>39</sup> Given the domination of triene  $S_1 \leftarrow S_0$

spectra by *cis*-isomers (their reduced symmetries presumably increase the  $S_1 \leftarrow S_0$  oscillator strength), the tetraene 2C-RE2PI spectrum was assigned to *cis,trans*-octatetraene, a minor component in the sample.<sup>39</sup> However, we subsequently obtained both the one- and two-photon fluorescence excitation spectra of octatetraene and were able to show that the major features of these spectra (and those of the 2C-RE2PI spectra) should be assigned to *trans,trans*-octatetraene.<sup>40</sup>

Even for the relatively simple, *trans,trans*-octatetraene,<sup>40</sup> the  $S_1 \leftarrow S_0$  spectrum is rather complex. A complete account could be given for the  $a_g$  and  $b_u$  in-plane modes, but we were unable to assign a number of relatively intense, low frequency bands, some of which must be due to out-of-plane vibrations. Such modes should not appear in the optical spectrum of a polyene with  $C_{2h}$  symmetry, and their presence may signal significant differences in the geometries of the  $S_1$  and  $S_0$  potential surfaces. Many of these bands also have anomalous lifetimes compared to the main bands. Since out-of-plane vibrations are involved in *cis-trans* isomerization, it will be important to assign these low-frequency bands as well as to understand their lifetimes and intensities.

The high fluorescence quantum yields of cold, isolated tetraenes give fluorescence excitation and emission spectra with excellent signal/noise ratios and allow accurate measurements of lifetimes of individual  $S_1$  vibronic levels. We report here the complete, one- and two-photon,  $S_1 \leftarrow S_0$  fluorescence excitation spectra and the  $S_1$  fluorescence lifetimes of the all-*trans* isomers of octatetraene, nonatetraene, and decatetraene in helium expansions. General features of the spectra of these three molecules are discussed, including their assignment to the  $2^1A_g \leftarrow 1^1A_g$  transitions of all-*trans*-polyenes. Analyses of these spectra leads to the accurate determination of electronic and vibronic origins and provides a detailed look at the effects of methyl substituents on electronic energies and lifetimes. The spectra also reveal the  $2^1A_g$  frequencies of the dominant C–C and C=C,  $a_g$  stretching modes and the low-energy, Herzberg–Teller,  $b_u$  promoting modes. We also are able to show that the characteristic splittings of the  $S_1 \leftarrow S_0$  spectra of nonatetraene and decatetraene are caused by the tunneling of terminal methyl groups through low torsional barriers in the  $2^1A_g$  states. Analysis of these splittings leads to a potential energy function for methyl rotation in  $2^1A_g$ . Finally, we provide a preliminary discussion of the fluorescence decay kinetics of  $S_1$  vibronic levels accessed by one- and two-photon excitation. This comprehensive survey of the  $2^1A_g$  states of isolated tetraenes provides the basis for studies of the excited states of more complicated polyenes and their dependence on substitution, length of conjugation, and external perturbations.

## II. EXPERIMENT

The preparation of tetraene samples and the apparatus for measuring one- and two-photon fluorescence excitation spectra, fluorescence lifetimes, and emission spectra have been described previously.<sup>36–38,40</sup> Nonatetraene and decatetraene were purified by recrystallization from hexane. Octatetraene is significantly less stable and was used directly as obtained from the dehydration step of a synthesis which ends with the collection of crystalline octatetraene in a dry ice

trap. All samples were stored as crystals at dry ice temperature. The decatetraene and octatetraene samples normally had only trace impurities, while nonatetraene had larger concentrations of *cis*-isomers. These isomers were depleted from the reservoir faster than all-*trans*-nonatetraene, so that useful jet spectra could be obtained even for samples that were not pure initially. The sample reservoir temperature was kept at  $<325$  K, which is sufficiently low to prevent significant isomerization or degradation. Helium stagnation pressures were 700–800 Torr for the one-photon spectra, and 500–600 Torr for the two-photon spectra.

The excimer-pumped, dye-laser excitation source<sup>40</sup> allowed lifetime measurements on  $\sim 10$  ns time scales. In order to measure fluorescence lifetimes at high  $S_1$  vibronic energies, the time resolution was improved by using a  $\sim 10$  ps excitation source and faster detection electronics. The laser system for these experiments was a Coherent 702 synchronously pumped dye laser, which operated with Rhodamine 6G dye and without a saturable absorber. The picosecond oscillator pulses were amplified at a 10 Hz repetition rate with a three-stage dye amplifier (Kiton Red or Sulforhodamine 640 dyes; tuning range of 585–625 nm) pumped by output from a Quantel regenerative amplifier. Use of a single plate birefringent filter in the oscillator resulted in a bandwidth of  $\sim 70$   $\text{cm}^{-1}$  after doubling with a BBO second harmonic crystal. This bandwidth was adequate since the  $S_1 \leftarrow S_0$  spectra are essentially structureless at high excitation energies. Excitation wavelengths were measured with a calibrated monochromator. Samples were excited by  $\sim 10$  ps,  $\sim 25$   $\mu\text{J}$  pulses with  $\sim 3$  mm beam diameter. Fluorescence was detected with a Hamamatsu Photonics H3284 photomultiplier (rise time of  $\sim 300$  ps). Fluorescence decays were recorded and averaged with a 11A79 vertical amplifier (1 GHz analog bandwidth) and a Tektronix 602A digitizing oscilloscope. This allowed accurate measurement of decays as short as 1 ns.

## III. RESULTS AND DISCUSSION

### A. Assignment of electronic and vibronic origins in $S_1 \leftarrow S_0$ spectra of all-*trans*-tetraenes

The one- and two-photon, fluorescence excitation spectra of the three polyenes near the  $S_1 \leftarrow S_0$  electronic origins are compared in Fig. 1. For octatetraene, the arguments for identifying the major features of the one- and the two-photon spectra with the *trans,trans*-isomer already have been discussed in considerable detail<sup>40</sup> and are based on vibronic analysis of the one- and two-photon  $S_1 \leftarrow S_0$  fluorescence excitation spectra, analysis of the hot-band structure of the one-photon excitation spectrum, analysis of  $S_1 \rightarrow S_0$  emission spectra from a range of vibronic levels, analysis of the  $S_2 \leftarrow S_0$  fluorescence excitation spectrum, and the fluorescence decay kinetics of individual  $S_1$  vibronic states. The most compelling evidence for the all-*trans* assignments is the large number of identical frequency intervals observed in the one- and two-photon spectra and the fact that vibronic levels accessed by one- and two-photon excitation have identical lifetimes in energy regions where intramolecular vibrational relaxation (IVR) couples levels of different symmetry.

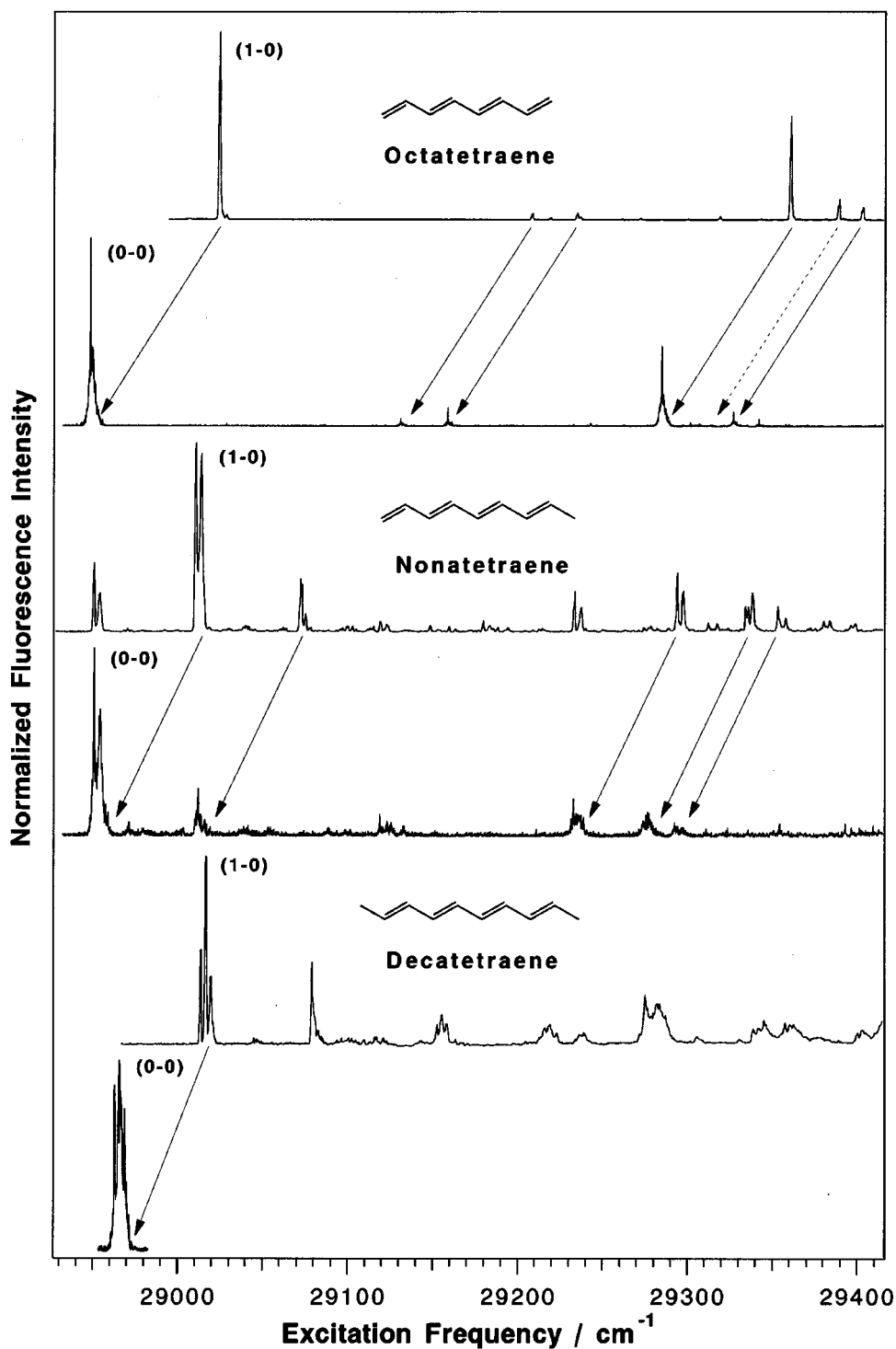


FIG. 1. Comparison of the origins of the one- and two-photon  $S_1 \leftarrow S_0$  fluorescence excitation spectra of all-*trans*-octatetraene, nonatetraene, and decatetraene. To emphasize that the one- and two-photon spectra of octatetraene and decatetraene do not overlap, the spectra are presented on an absolute energy scale (observed transition energies). Spectra have been normalized to give the same intensities for the electronic and vibronic origins of each molecule. Full arrows indicate bands that build on both electronic and vibronic origins. The broken arrow indicates a  $b_u$  band that only is observed in the one-photon spectrum.

### B. One-photon $S_1 \leftarrow S_0$ spectra of all-*trans*-tetraenes

Complete one-photon fluorescence excitation spectra of the  $2^1A_g \leftarrow 1^1A_g$  transitions and the fluorescence decay rates of  $2^1A_g$  vibronic levels of all-*trans*-octatetraene, nonatetraene, and decatetraene are shown in Fig. 2. The energies of the electronic and vibronic origins are summarized in

Table I. The complex vibrational development of the one-photon spectra is due to the presence of several  $b_u$  ( $1 \leftarrow 0$ ) vibronic origins, reflecting the symmetry-forbidden nature of the  $2^1A_g \leftarrow 1^1A_g$  transitions. The fluorescence decay rates for vibronic levels accessed by one-photon excitation range from  $2.9 \times 10^6 \text{ s}^{-1}$  ( $\tau = 350 \text{ ns}$ ) at the vibronic origins to

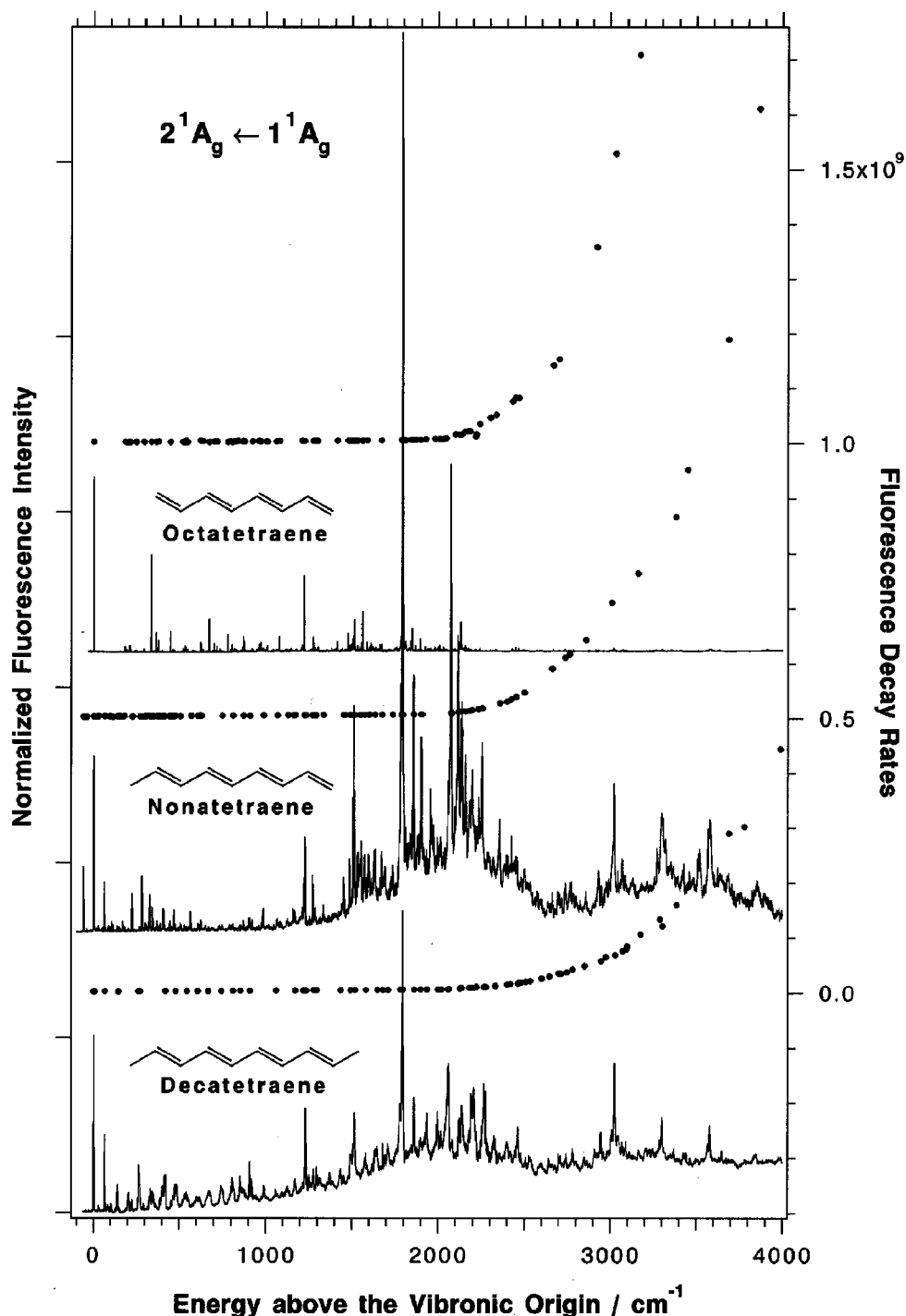


FIG. 2. Comparison of one-photon  $S_1 \leftarrow S_0$  fluorescence excitation spectra and fluorescence decay rates of all-*trans*-octatetraene, nonatetraene, and decatetraene. For purposes of comparing vibronic structure, the lowest energy vibronic origin ( $b_u$ ) is taken as the zero of energy for each molecule. The right ordinate gives the decay rates for the vibronic levels of decatetraene. The decay rates for nonatetraene and octatetraene are displaced by  $0.5 \times 10^9 \text{ s}^{-1}$  and  $1.0 \times 10^9 \text{ s}^{-1}$ , respectively.

$> 1 \times 10^9 \text{ s}^{-1}$  ( $\tau < 1 \text{ ns}$ ) at the high energy limits of the measurements. The overall similarities between spectra (including the energies of the electronic origins, Table I) and fluorescence decay rates for the three molecules indicate that terminal methyl groups do not greatly perturb tetraene  $S_0$  and  $S_1$  electronic states.

The one-photon,  $2^1A_g \leftarrow 1^1A_g$  fluorescence excitation spectrum of octatetraene is dominated by sharp vibrational

bands, most of which can be assigned to  $b_u$  Herzberg–Teller promoting modes and their combination bands with  $a_g$  modes. Intensities of these bands are governed by the strength of  $S_2$ – $S_1$  coupling induced by different  $b_u$  vibrations, Franck–Condon factors (largest for modes involving CC stretching), and fluorescence quantum yields that decrease with increasing excitation energy. Preliminary assignments for the octatetraene spectrum were presented in Ref.

TABLE I. Comparison of one- and two-photon origins of tetraenes. Energies and frequencies are in  $\text{cm}^{-1}$ , lifetimes are in ns. Vibrational frequencies refer to  $2^1A_g$  state.

Molecule	Two-photon origin (lifetime)	One-photon origin (lifetime)	In-plane bending frequency ( $b_u$ )	C–C stretching frequency ( $a_g$ )	C=C stretching frequency ( $a_g$ )	CH <sub>3</sub> tunneling splitting
<i>trans,trans</i> -octatetraene	28 948.7 (446)	29 024.9 (341)	76.2	1225	1798	...
<i>all-trans</i> -nonatetraene	28 950.8 (346)	29 010.9 (287)	60.1	1229	1793	3.5
<i>all-trans</i> -decatetraene	28 963.1 (487)	29 014.0 (344)	50.9	1231	1793	3.2

40. Nonatetraene also exhibits many sharp bands, though the absence of inversion symmetry and the excitation of methyl torsional modes significantly complicates its  $S_1 \leftarrow S_0$  spectrum. Even though decatetraene shares octatetraene's  $C_{2h}$  symmetry, its spectrum is considerably more complex. The significantly higher density of vibrational states contributed by methyl torsions results in increased spectral congestion. For vibronic energies  $>200 \text{ cm}^{-1}$  above the vibronic origin there are no isolated bands, and above  $\sim 500 \text{ cm}^{-1}$  these bands coalesce into clumps of irregular line shapes with widths of  $7\text{--}25 \text{ cm}^{-1}$ .<sup>37</sup> The methyl substituted tetraenes have a continuous absorption background at higher excitation energies. This most likely is due to the higher density of states and strong coupling between the methyl torsions and low frequency skeletal modes. For all three tetraenes, transitions involving the C–C and C=C stretching modes ( $\sim 1225 \text{ cm}^{-1}$  and  $\sim 1795 \text{ cm}^{-1}$ , respectively, see Table I) have the largest Franck–Condon factors and strongest intensities. This characteristic signature of polyene spectroscopy is due to the redistribution of CC bond-orders upon  $2^1A_g \leftarrow 1^1A_g$  excitation.

For isolated tetraenes there is a rapid decrease both in fluorescence intensity and in spectral structure above  $\sim 2000 \text{ cm}^{-1}$  excess vibronic energy. No resolvable structure is observed above  $4300 \text{ cm}^{-1}$ . This contrasts the spectra of mixed crystal systems for which the intensities of tetraene  $S_1 \leftarrow S_0$  fluorescence excitation spectra systematically increase up to the  $S_2 \leftarrow S_0$  origins.<sup>12,21,24,26</sup> In jets, the  $S_1 \rightarrow S_0$  emission spectra show maximum vibronic intensities at two or three quanta of the C=C stretch, while the  $S_1 \leftarrow S_0$  fluorescence excitation spectra have intensity maxima at one quantum of the C=C stretch. These differences are due to the competition between  $2^1A_g$  fluorescence and nonradiative decay processes with activation energies of  $2000\text{--}2100 \text{ cm}^{-1}$ . These decay channels are most evident from the energy dependence of the fluorescence lifetimes.

### C. Two-photon $S_1 \leftarrow S_0$ spectra of all-*trans*-tetraenes

The two-photon fluorescence excitation spectra and fluorescence lifetimes of octatetraene and nonatetraene are compared with the one-photon spectra and lifetimes in Figs. 3 and 4. The two-photon spectrum of decatetraene is significantly weaker, and we only have been able to measure the triplet of bands at the origin (Fig. 1). For decatetraene, the  $2^1A_g \leftarrow 1^1A_g$  oscillator strength is distributed over many more vibronic bands due to interactions between methyl torsions and low frequency skeletal modes (see Sec. III D). The combination of broad, unresolved bands and its lower vapor pressure made it difficult to obtain the two-photon spectrum

of decatetraene in our experiment. The two-photon spectra of all three polyenes are symmetry allowed, and their vibronic development consists only of progressions of  $a_g$  vibronic bands. As discussed in the previous section, the one-photon spectra are considerably more complex, since the vibronic development of  $a_g$  bands builds on several  $b_u$  vibronic origins. The relatively simple progressions in  $a_g$  modes in the two-photon spectra thus provide convenient templates for identifying bands associated with each vibronic origin in the one-photon spectra. The lack of overlap of the one- and two-photon spectra and the excellent agreement between  $a_g$  frequencies observed in the spectra reinforce our conclusion that all-*trans* isomers are responsible for the dominant features of Figs. 3 and 4.

Comparison of the origins of the one- and two-photon spectra of the three tetraenes (Fig. 1) highlights the forbidden nature of the  $2^1A_g \leftarrow 1^1A_g$  one-photon transitions. The frequencies and lifetimes of the one- and two-photon origins are given in Table I. Note that methyl-substitution shifts the electronic origins to higher energy by only 2.1 and  $14.4 \text{ cm}^{-1}$ , respectively, for nonatetraene and decatetraene. The origin of the two-photon spectrum is the electronic origin (0–0) of the  $2^1A_g \leftarrow 1^1A_g$  transition, while the origin of the one-photon spectrum is a vibronic origin (1–0) corresponding to the excitation of one quantum of the lowest frequency  $b_u$  in-plane bending vibration. Other  $b_u$  vibronic origins also can be easily identified in Figs. 3 and 4. The  $a_g$  bands appearing in the two-photon spectra are displaced in the one-photon spectra by the frequencies of the different  $b_u$  vibronic origins. Shifted  $a_g$  bands and  $b_u$  bands missing in the two-photon spectrum of octatetraene are indicated in Fig. 1.

Nonatetraene lacks inversion symmetry, resulting in considerable overlap between its one- and two-photon spectra. As shown in Figs. 1 and 3, the most intense band in the origin region of the one-photon spectrum of nonatetraene occurs at  $60.1 \text{ cm}^{-1}$ , at approximately the same energy as the vibronic origins of octatetraene and decatetraene. This band most likely corresponds to the lowest frequency in-plane bending mode, which gains intensity by  $S_2 \leftarrow S_1$  vibronic coupling. The significantly higher intensity of the vibronic origin with respect to the electronic origin indicates that Herzberg–Teller vibronic coupling is a dominant factor in determining the strength of polyene electronic transitions, even in molecules without rigorous inversion symmetry. The relative contribution of vibronic coupling to the transition moment is even more pronounced at higher excitation energies. For instance, while the ratio of peak intensities of the electronic and vibronic origins is  $\sim 0.4$ , the ratio drops to 0.04 for the C=C stretch fundamental and the corresponding combina-

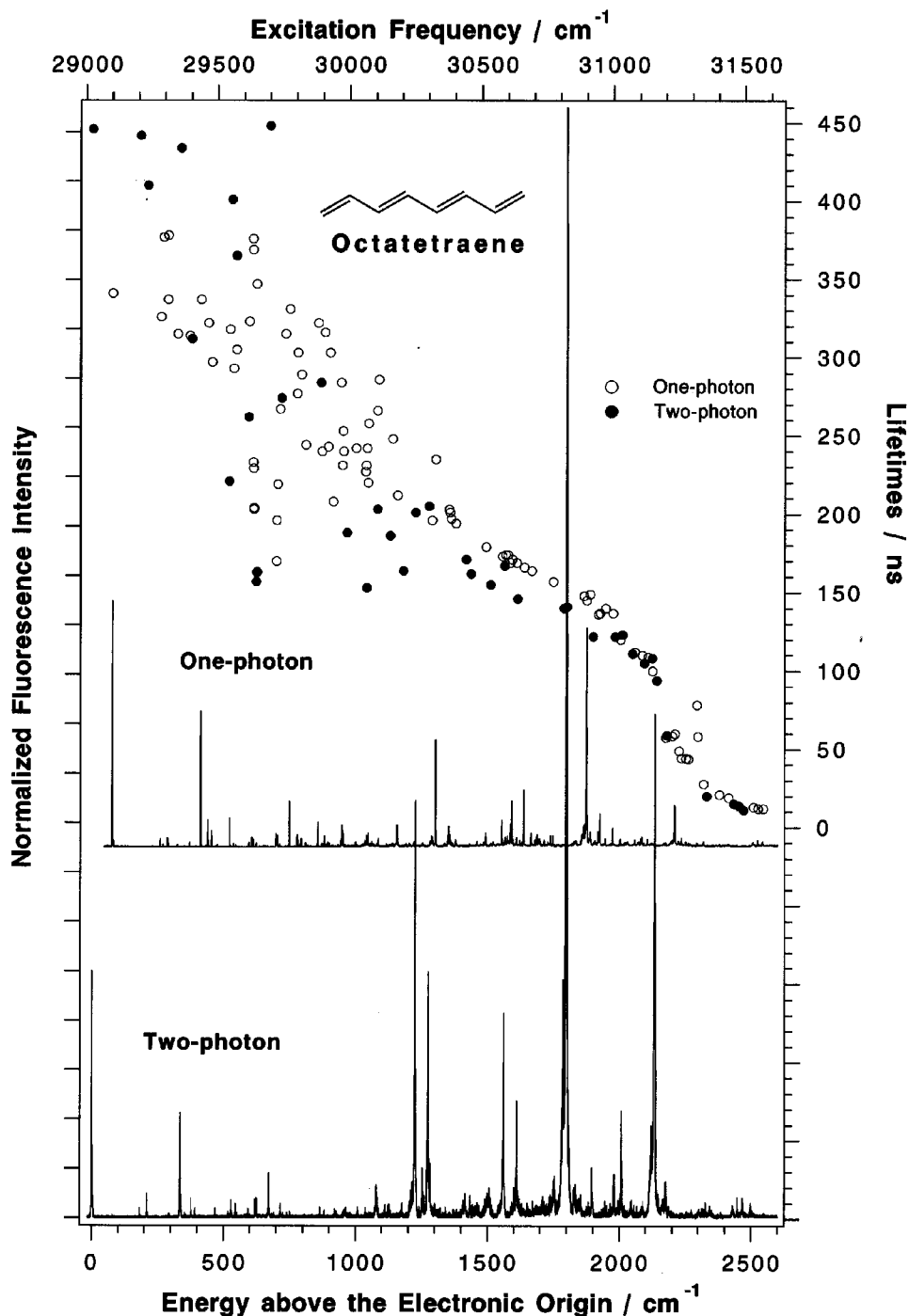


FIG. 3. One- and two-photon  $S_1 \leftarrow S_0$  fluorescence excitation spectra and fluorescence lifetimes of *trans,trans*-octatetraene. The right ordinate has been displaced for clarity. The two-photon spectra have not been normalized for the variations in laser power. Relative intensities thus are given only as a qualitative guide.

tion band. [It is interesting to note that an almost identical ratio ( $\sim 0.04$ ) is observed for octatetraene in a variety of *n*-alkane mixed crystals that distort its  $C_{2h}$  symmetry.<sup>28</sup>] The majority of the bands in the one-photon, jet spectrum of non-atetraene (and of all-*trans* polyenes in condensed phases) thus derive their intensity from Herzberg–Teller coupling. Also, it should be noted that even though the lowest-frequency, in-plane bending mode could appear in the two-photon spectrum, it is either quite weak or not observable,

due to interference from a methyl torsion band with an almost identical frequency.

Although the two-photon spectral intensities have not been normalized for the laser power, most of the main bands have relative intensities comparable to progressions seen in the one-photon spectra. A few weak bands that appear in the two-photon excitation spectra but which are not observed for one-photon excitation may be due to impurities. At higher resolution the rotational band profiles for one- and two-

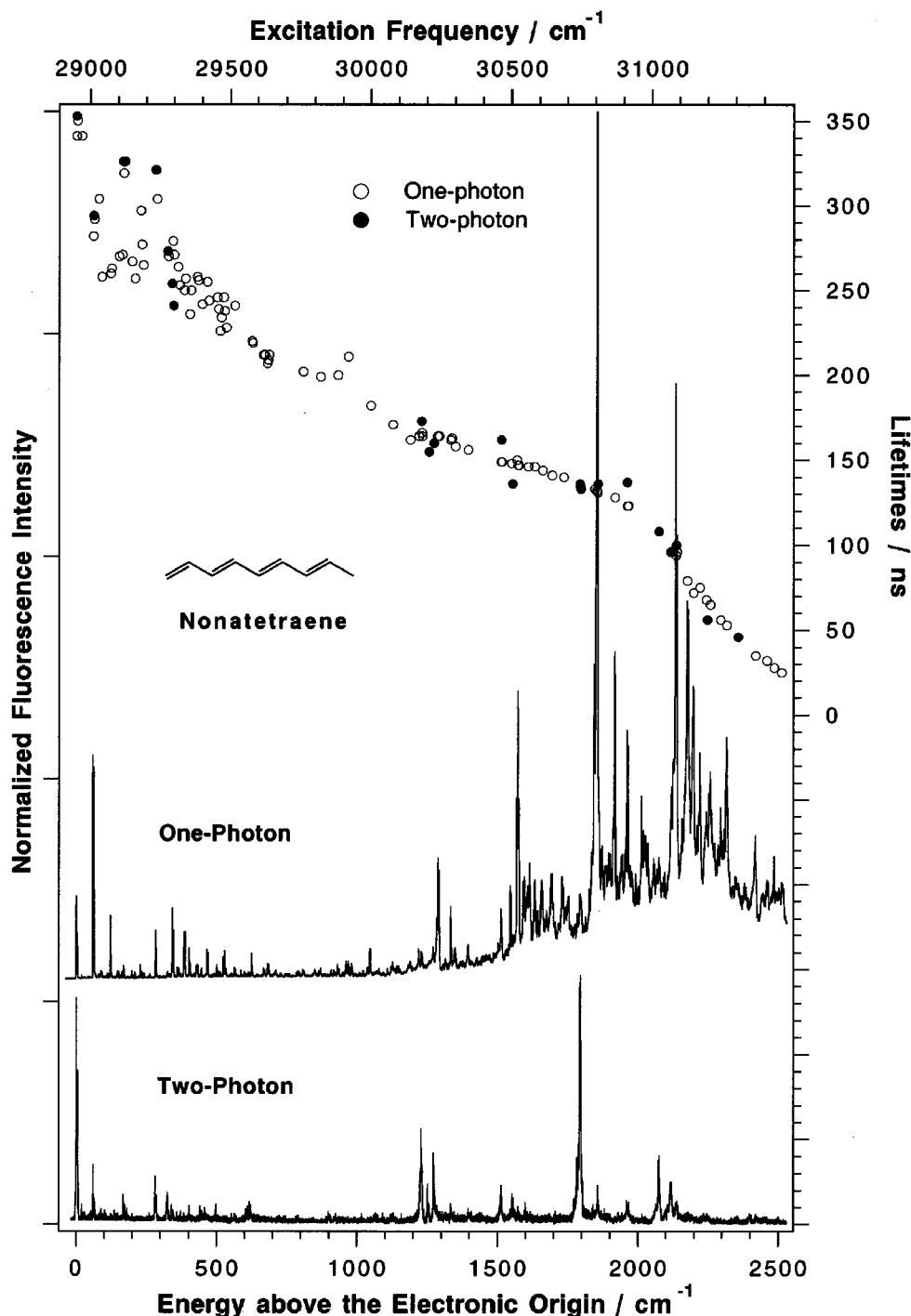


FIG. 4. One- and two-photon  $S_1 \leftarrow S_0$  fluorescence excitation spectra and fluorescence lifetimes of all-*trans*-nonatetraene. The right ordinate has been displaced for clarity. The two-photon spectra have not been normalized for the variations in laser power. Relative intensities thus are given only as a qualitative guide.

photon spectra are significantly different. The breadth of the two-photon bands is due in part to the higher rotational temperatures of these spectra, resulting from lower stagnation pressures. More importantly, the rotational selection rules are different for one- and two-photon spectra. For parallel transitions, one-photon spectra have *P* and *R* branches, whereas two-photon spectra have *O*, *P*, *Q*, *R*, and *S* branches. The sharp central peaks in two-photon spectra are due to *Q*-branches and the broad pedestals are due to overlapping

$\Delta J \neq 0$  transitions. Although the *Q*-branches clearly stand out in octatetraene, this is not the case for most vibronic bands of the methyl-substituted tetraenes.

#### D. Effects of methyl torsions on the $S_1 \leftarrow S_0$ spectra of nonatetraene and decatetraene

The  $S_1 \leftarrow S_0$  spectra of decatetraene and nonatetraene are significantly complicated by their terminal methyl groups.

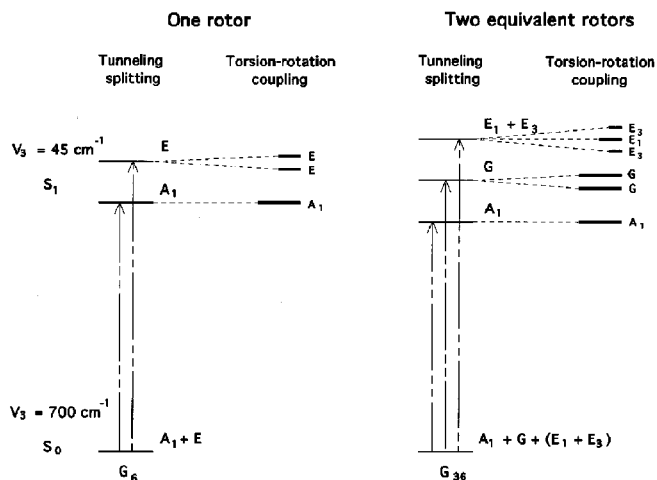


FIG. 5. A schematic diagram showing the splitting of the nonatetraene (one rotor) and decatetraene (two rotors) origins due to methyl torsion and torsion-rotation interactions.

This is particularly noticeable at the origins (Fig. 1); for octatetraene the origin is a singlet, for nonatetraene a doublet, and for decatetraene a triplet. The splittings observed for nonatetraene and decatetraene are  $3.2\text{--}3.5\text{ cm}^{-1}$ . In addition to the splitting of the origins and other vibronic bands, additional bands due to excitation of one or more quanta of the methyl torsion are observed at higher energy. Comparison of the octatetraene  $2^1A_g \leftarrow 1^1A_g$  spectrum with those of nonatetraene and decatetraene helps to identify bands due to methyl torsions.

The splittings of bands in the  $S_1 \leftarrow S_0$  spectra of the methyl-substituted tetraenes are due to the tunneling of methyl groups through low torsional barriers in the  $S_1$  states. The potential energy for internal rotation of a single methyl group in a planar molecule is given by a truncated Fourier series in the torsional angle  $\Phi$ ,<sup>41,42</sup>

$$V(\Phi) = 1/2 V_3 (1 - \cos 3\Phi) + 1/2 V_6 (1 - \cos 6\Phi).$$

When  $|V_3/V_6| > 4$ , the torsional potential has minima at  $\Phi = 0^\circ, 120^\circ$ , and  $240^\circ$ . For the electronic ground states of simple, methyl-substituted olefins, aldehydes, and ketones (e.g., propene and acetaldehyde), these minima correspond to conformations with a C–H bond syn or “eclipsed” to the double bond.<sup>43,44</sup> When  $|V_3/V_6| < 4$ , the potential has six minima with positions depending on the ratio  $V_3/V_6$ . For high torsional barriers, the states bound in the potential are triply degenerate. Low energy barriers lift the degeneracy leading to observable fine structure in the spectra (Fig. 5). In the limit of free methyl rotation ( $V_3$  and  $V_6 = 0$ ) these splittings will appear as certain multiples of the rotational constant for the methyl rotor ( $\sim 5\text{ cm}^{-1}$ ).<sup>45</sup>

Solving the Schrödinger equation with the above potential function yields energy levels that can be labeled by the rotational quantum numbers for the one-dimensional free rotor and irreducible representations of the permutation inversion group ( $G_6$ ) isomorphous to the  $C_{3v}$  point group.<sup>46,47</sup> The labels used are  $a_1$ ,  $a_2$ , and  $e$ . Singly degenerate  $a_1$  and  $a_2$  levels can be considered as torsional vibrations while the  $e$  levels arise from the vibrational plus rotational components

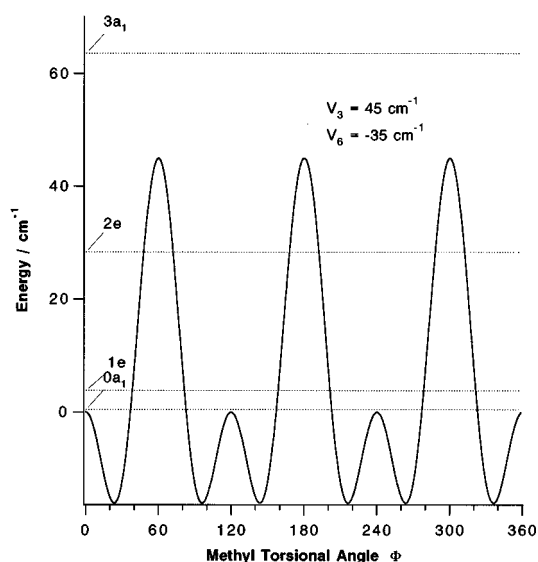


FIG. 6. Potential energy and lowest energy levels for the hindered internal rotation of the  $\text{CH}_3$  group in the  $S_1$  state of nonatetraene.  $V_3 = 45 \pm 10\text{ cm}^{-1}$ ,  $V_6 = -35 \pm 4\text{ cm}^{-1}$ , and the zero-point energy  $= 0.43\text{ cm}^{-1}$ .

of motion. Selection rules governing transitions between the methyl rotor levels are  $a_1 \leftarrow a_1$ ,  $a_2 \leftarrow a_2$ , and  $e \leftarrow e$ .

We have calculated splittings in the  $S_1 \leftarrow S_0$  spectra of nonatetraene, assuming that the ground state potentials of methyl-substituted tetraenes are the same as that of propene ( $V_3 = 700\text{ cm}^{-1}$  and  $V_6 = -12\text{ cm}^{-1}$ ).<sup>48</sup> The large value of  $V_3$  results in a negligible splitting ( $\ll 0.3\text{ cm}^{-1}$ ) of the  $v'' = 0$  ( $0a_1$  and  $1e$ ) rotor levels [Fig. 5(a)]. The ground state values for  $V_3$  and  $V_6$  thus have little effect on the  $2^1A_g \leftarrow 1^1A_g$  transition frequencies. Keeping the ground state values constant, we varied the upper state parameters and obtained a best fit with  $2^1A_g$  values of  $V_3 = 45 \pm 10\text{ cm}^{-1}$ ,  $V_6 = -35 \pm 4\text{ cm}^{-1}$ . The observed splittings thus point to a dramatic reduction in the barrier to methyl rotation upon excitation to the  $S_1$  state. The methyl torsional potential energy surface derived from these parameters is shown in Fig. 6. Since  $|V_3/V_6| < 4$ , the potential has six minima, and these are displaced by approximately  $24^\circ$  on either side of the minima at  $0^\circ, 120^\circ$ , and  $240^\circ$  for the  $1^1A_g$  state. Figure 6 also gives the energies of the lowest four torsional states including a calculated zero point energy of  $0.43\text{ cm}^{-1}$ . Assignments of the one-photon nonatetraene spectrum in the regions of the electronic and the vibronic origins are given in Fig. 7 and a comparison of the calculated and observed transition energies is provided in Table II. The next highest methyl rotor levels in the  $1^1A_g$  state, the almost degenerate  $2e$  and  $3a_2$  ( $v'' = 1$ ) levels, are approximately  $170\text{ cm}^{-1}$  above the zero-point levels. Given the low temperatures of the molecular beams, the populations of these levels should be more than an order of magnitude lower than those of the  $0a_1$  and  $1e$  rotor levels, and we have ignored their contribution to the  $2^1A_g \leftarrow 1^1A_g$  spectra. The relative magnitudes of the  $V_6$  and  $V_3$  terms in the  $2^1A_g$  state and the significant deviations between calculated and observed energies imply that additional terms in the potential energy expansion are required to accurately describe the methyl torsional potential in nonatetraene.

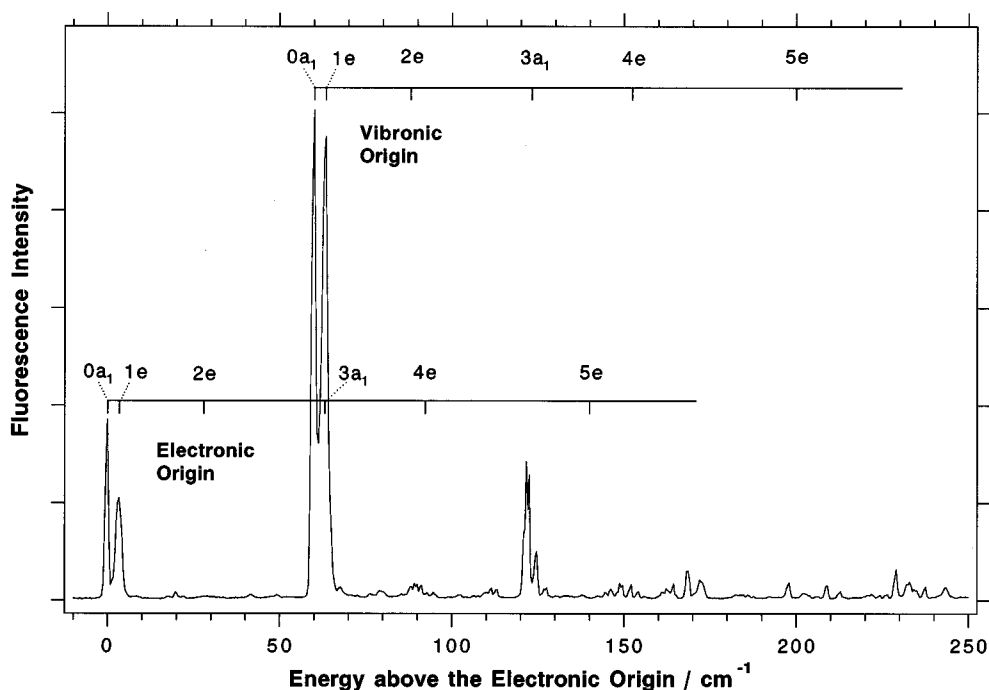


FIG. 7. The origin region of the one-photon  $S_1 \leftarrow S_0$  fluorescence excitation spectrum of nonatetraene. Both the electronic and vibronic origins are observed for nonatetraene, as expected for a noncentrosymmetric molecule. The calculated positions of a number of low frequency modes due to methyl torsions are shown. The symmetry labels correspond to the  $S_1$  state.

raene. However, we have not observed a sufficient number of torsional states to reliably determine the coefficients of higher order terms.

The equilibrium conformation of the methyl group in the electronic ground state is determined by the balance of repulsive interactions between filled  $\pi$ -symmetry orbitals on the methyl group and polyene framework and attractive interactions between the occupied and unoccupied  $\pi$  orbitals. For propene, Dorigo and co-workers<sup>44</sup> have calculated that the repulsion between filled  $\pi$   $\text{CH}_3$  and  $\pi$   $\text{C}=\text{C}$  orbitals is minimum, and the attraction between  $\pi$   $\text{CH}_3$  and the vacant  $\pi^*$   $\text{C}=\text{C}$  orbitals is maximum for the eclipsed conformation of the  $S_0$  state. In the first excited triplet state of propene these interactions involve only three electrons and apparently are not important in determining the most stable conformation.<sup>44</sup> However, the attractive interactions between

the vacant  $\pi^*$   $\text{CH}_3$  and singly occupied  $\pi^*$   $\text{C}=\text{C}$  orbitals favor the staggered conformation, and this is thought to be the primary reason for the  $\sim 450 \text{ cm}^{-1}$  preference for this conformer in the lowest energy,  $^3\pi\pi^*$  state.<sup>44</sup> Similar effects may contribute to the stabilization of staggered forms in the  $2^1A_g$  states of linear polyenes, though the barrier is determined by several competing interactions and difficult to attribute it to any single effect. Preliminary *ab initio* calculations predict that in  $2^1A_g$  the eclipsed form of decatetraene is more stable than the staggered form by  $\sim 100 \text{ cm}^{-1}$ , in reasonable agreement with experiment.<sup>49</sup> However, further theoretical work will be required to better understand the source(s) of the low barrier to methyl torsions in polyene  $2^1A_g$  states.

For decatetraene we assume that the two methyl rotors act independently and that the resulting levels can be represented by combinations of the single methyl case. The effect of each methyl group is identical, and the origin is split into a triplet with a 1:2:1 intensity ratio. Figure 5(b) is labeled using the  $G_{36}$  permutation group. Applying the potential parameters determined for nonatetraene to the two-methyl case gives an excellent match with the observed splittings of the decatetraene origin. We also were able to fit a number of low frequency bands. However, intensities cannot be simulated in this approach, and it proves difficult to unambiguously assign these lines. The selection rules for methyl rotor transitions ensure that transitions between the  $a_1$  and  $e$  levels are forbidden. For nonatetraene this results in “independent” spectra from two noninterconvertible forms of the same molecule. Similarly, we expect three forms for decatetraene. We have shown this to be the case for nonatetraene and decatet-

TABLE II. Observed and calculated methyl rotor energy levels for nonatetraene. (Energies relative to 1- and 2-photon  $2^1A_g \leftarrow 1^1A_g$  origins are in  $\text{cm}^{-1}$ .)

$2^1A_g$ state rotor levels	2-photon origin			1-photon origin	
	Calculated	Observed	Observed-calculated	Observed	Observed-calculated
$0a_1$	0.00	0.00	0.00	0.00	0.00
$1e$	3.38	3.34	-0.04	3.37	-0.01
$2e$	27.92	20.54	-7.38	19.81	-8.11
$3a_1$	63.17	$\sim 61^a$	$\sim -2.17$	61.62	-1.55
$4e$	92.26	91.27	-0.99	92.17	-0.09
$5e$	139.94	144.55	4.61	138.06	-1.88

<sup>a</sup>Line position is approximate due to overlap with the one photon origin.

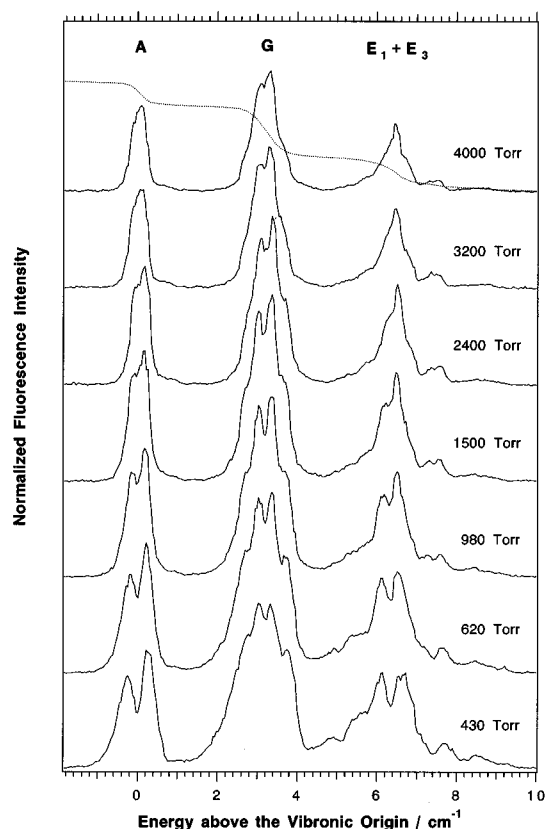


FIG. 8. Effect of helium seeding gas pressure on the rotational contours for the A, G, and  $E_1 + E_2$  bands of the decatetraene vibronic origin. Dotted line shows integrated intensities at 4000 Torr backing pressure and confirms the expected 1:2:1 ratio for the triplet origin.

raene by producing very cold samples in the molecular beam and observing that the relative intensities of the multiple origin lines are independent of temperature (Fig. 8).

Figure 9 shows the high resolution ( $0.005 \text{ cm}^{-1}$ ) spectra of the octatetraene, nonatetraene, and decatetraene one-photon vibronic origins. The octatetraene band shape is determined solely by its rotational temperature and can be simulated by a parallel transition of a classic prolate symmetric top. The parameters used to get this fit are  $A'' = 0.619 \text{ cm}^{-1}$ ,  $B'' = C'' = 0.020 \text{ cm}^{-1}$ ,  $A' = 0.670 \text{ cm}^{-1}$ ,  $B' = C' = 0.019 \text{ cm}^{-1}$ . The ground state rotational constants were calculated from the theoretical structure<sup>49</sup> and the excited state constants were varied to reproduce the observed rotational envelope. This fit gives a rotational temperature of 55 K for the expansion conditions used (nozzle temperature = 300 K, backing pressure 400 Torr He).

The substructure observed in the A symmetry levels of nonatetraene and decatetraene spectra are very similar to that of octatetraene. As the rotational temperature decreases, the band profiles collapse into unresolved P and R branches. However, for the E and G bands of nonatetraene and decatetraene there is additional structure, which cannot be removed by cooling. At the highest nozzle pressures (greatest cooling) we still observe structure in the second and third members of the triplet (Fig. 8). Similar effects have been encountered in the fluorescence excitation spectrum of 2,3-dimethylnaphthalene<sup>50</sup> and were assigned to torsion-

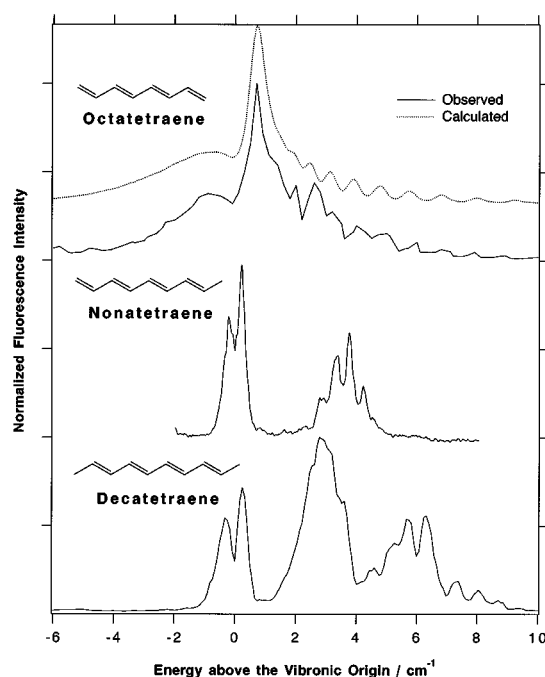


FIG. 9. High resolution one-photon fluorescence excitation spectra of the vibronic origins of octatetraene, nonatetraene, and decatetraene. The calculation of the rotational envelope for octatetraene (nozzle temperature=300 K, backing pressure=400 Torr He) is described in the text.

rotation interaction of the two methyl groups. In the absence of torsion-rotation interaction, the rotational band shapes will be identical and the origin will split into a 1:2:1 pattern of intensities [Fig. 5(b)]. However, with torsion-rotation interaction the G level splits into a doublet and the  $E_1 + E_3$  level splits into a triplet with an intensity ratio of 1:2:1 [Fig. 5(b)]. The coldest spectrum of decatetraene suggests the presence of such features, though the limited resolution of our experiment prevented a more detailed investigation. A large torsion-rotation splitting is a direct consequence of the low torsional barrier in the  $2^1A_g$  state. The effect of this additional splitting also can be seen in the two-photon spectra, which have sharp Q-branches. For E and G states of nonatetraene and decatetraene, the Q-branches should be even better resolved than the P and R-branches in the one-photon spectra. However, due to the poor signal to noise ratio of the two-photon spectra, we have not been able to observe this effect.

### E. Lifetimes of the $2^1A_g$ states of isolated tetraenes

Excited state lifetimes provide information on the radiative and nonradiative pathways by which polyenes dispose of their electronic and vibrational energies. The dependence of these processes on substituents, conjugation length, and molecular geometry are issues of fundamental importance for understanding polyene photochemistry. Radiative and nonradiative decays both depend on vibronic coupling between the lowest energy electronic states. The ability of supersonic expansions to produce rotationally and vibrationally cool polyenes under collision-free conditions allows the measurement of the kinetics of individual vibronic levels both as a func-

tion of their symmetries (one- and two-photon experiments access different vibronic levels) and total vibronic energy.

The  $2^1A_g \rightarrow 1^1A_g$  fluorescence lifetimes of octatetraene and decatetraene are  $\sim 450$  and  $\sim 490$  ns for emission from the electronic origins ( $a_g$  vibronic symmetry) and  $\sim 350$  ns for emission from the vibronic origins ( $b_u$  vibronic symmetry). These lifetimes are the longest yet observed for linear polyenes. The difference between lifetimes of the electronic and vibronic origins is due to the fact that  $2^1A_g \rightarrow 1^1A_g$  transitions from  $b_u$  vibronic states derive their transition moments from  $1^1B_u - 2^1A_g$  coupling, whereas the transition moments from  $a_g$  vibronic states depend on  $1^1B_u - 1^1A_g$  coupling. The longer lifetimes of  $a_g$  vibronic bands (e.g., the electronic origin) is consistent with weaker  $S_2 - S_0$  couplings due to the larger  $S_2 - S_0$  energy gap. For octatetraene, systematic differences between the lifetimes of vibronic levels accessed by one and two photon excitation ( $b_u$  and  $a_g$  symmetries) persist up to  $\sim 1000$   $\text{cm}^{-1}$  excess energy (Fig. 3). At higher vibrational energies intramolecular vibrational redistribution (IVR) becomes sufficiently fast to randomize the excitation energy among modes of different symmetry. This results in *average* lifetimes that depend only on the excitation energy rather than on the symmetry of the vibronic state. Similar effects have been seen in the one- and two-photon  $2^1A_g \leftarrow 1^1A_g$  spectra of diphenylbutadiene, for which the fluorescence lifetime is approximately three times longer at the electronic origin ( $a_g$ ) than at the vibronic origin ( $b_u$ ).<sup>51</sup> The more modest differences between the lifetimes of  $a_g$  and  $b_u$  vibronic levels in the  $2^1A_g$  state of octatetraene may be a consequence of systematic differences between  $S_2 - S_0$  and  $S_1 - S_0$  coupling strengths and/or differences in the rates of radiationless decay from the  $a_g$  and  $b_u$  levels. Understanding the effects of nonradiative processes on lifetimes awaits measurements of relative fluorescence quantum yields.

The shorter fluorescence lifetimes of all-*trans*-nonatetraene reflect its reduced symmetry. Even though  $a_g$  and  $b_u$  labels for in-plane vibrations are not strictly valid, lifetimes still depend on the approximate symmetry. The one- and two-photon spectra are distinctly different, and lifetimes of bands built on the lowest frequency vibronic origin are systematically (10%–20%) shorter than those built on the electronic origin (Fig. 4). These differences persist up to  $\sim 400$   $\text{cm}^{-1}$  excess energy, above which average lifetimes again are observed due to IVR. The methyl groups in nonatetraene and decatetraene increase the density of vibrational states and most likely introduce additional mechanisms for vibrational mode coupling, both of which promote IVR at lower energies than in octatetraene. Though the differences in lifetimes disappear at high excess energies, bands due to Herzberg–Teller coupling dominate the  $S_1 \leftarrow S_0$  excitation spectrum (Fig. 4). The relatively short lifetimes of bands built on vibronic origins reinforce the conclusion that Herzberg–Teller vibronic coupling often is the dominant factor in determining the strength of polyene  $S_1 \leftrightarrow S_0$  transitions, even in molecules without inversion symmetry. This also explains why *cis* and *trans* isomers of octatetraene have comparable  $S_1 \rightarrow S_0$  fluorescence lifetimes in low temperature mixed crystals.<sup>23,40,52,53</sup>

The fluorescence decay rates of the three tetraenes point

to a common nonradiative decay process with an activation energy of  $\sim 2100$   $\text{cm}^{-1}$ . We have tentatively attributed this to *trans*–*cis* isomerization about one of the central  $\text{C}=\text{C}$  bonds. As noted previously (see Fig. 2), above the  $2100$   $\text{cm}^{-1}$  threshold nonradiative decay at a given excess energy is fastest for octatetraene, resulting in fluorescence quantum yields that are significantly smaller than those of the methyl substituted tetraenes. In the limit that the vibrational energy is statistically distributed, the activated nonradiative decay rate should be inversely proportional to the density of vibrational states. Differences in nonradiative decay rates, and the relatively sharp onset of nonradiative decay in octatetraene, thus can be explained by the contribution of methyl groups to the total density of states. We recently completed a more-detailed study on the rate of isomerization of octatetraene as a function of vibrational energy near the  $2100$   $\text{cm}^{-1}$  threshold.<sup>54</sup> Stepwise increases in the isomerization rate with increasing energy indicate quantization of the vibrational levels of the transition state leading to *cis*–*trans* isomerization. A complete description of the isomerization of isolated octatetraene and a quantitative comparison with the RRKM theory for unimolecular reactions will be presented in a subsequent paper.

## F. *cis*-tetraenes

Most of the bands in the Figs. 1–4 are due to all-*trans* isomers. To understand the effect of the loss of inversion symmetry on  $2^1A_g \leftarrow 1^1A_g$  transitions and to more accurately define the potential surface for *cis*–*trans* isomerization, it will be necessary to investigate *cis*-tetraenes in supersonic jets. Unfortunately, pure *cis*-isomers are not available in the amounts required to do jet experiments and only have been studied as impurities in samples dominated by all-*trans* species. Studies by Kohler and co-workers on octatetraene isomers in mixed crystals show that relative to *trans*, *trans*-octatetraene, the  $S_1 \leftarrow S_0$  origins of *cis*-isomers tend to appear at lower energies,  $\sim 1000$   $\text{cm}^{-1}$  less for *s-cis* isomers, and  $\sim 100$   $\text{cm}^{-1}$  less for *cis* isomers.<sup>23,24,25</sup>

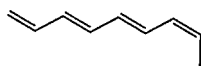
Due to the higher levels of *cis* impurities in nonatetraene, its fluorescence excitation spectra have provided the most detailed information on *cis*-isomers. The origins and several low frequency bands of at least two nonatetraene *cis*-isomers were determined by measuring spectra of several samples at different reservoir temperatures. Identification of these bands with impurities is supported by the variation of their intensities with respect to those of the main bands from sample-to-sample and during the course of experiments. As samples were depleted, the intensities of peaks due to impurities decreased more rapidly than those of the all-*trans*-isomer, suggesting that *cis*-isomers have higher vapor pressures and/or are less stable. The intensity of these bands probably overestimates the concentration of impurities in the samples, because *cis*-isomers are expected to have larger  $S_1 \leftarrow S_0$  transition moments. Several *cis*-isomers bands and their lifetimes are listed in Table III.

Analysis of these spectra identifies one isomer with an electronic origin  $18.0$   $\text{cm}^{-1}$  below the origin of the all-*trans*-isomer. A vibronic origin, presumably the counterpart of  $60.1$   $\text{cm}^{-1}$   $b_u$  vibration seen for all-*trans*-nonatetraene, appears

TABLE III. The frequencies, intensities, and lifetimes of bands assigned to *cis*-isomers of nonatetraene.

Isomer	Frequency/cm <sup>-1</sup>	Intensity	Lifetime/ns
<i>cis</i> I	0.0(28 932.8)	100	
	2.5	110	
	58.8	245	
	60.9	217	
	120.3	19	
	101.7	7	
<i>cis</i> IIa	0.0(28 865.5)	100	233
	1.7	89	236
	65.2	23	215
	67.3	20	
	100.4	7	
	101.7	7	
	125.6	7	
	127.7	7	
	158.1	7	
	286.1	41	
	290.6	70	197
	294.0	24	
	343.4	23	
	345.6	23	
	348.1	13	
	350.7	14	
	353.7	9	
370.8	13		
372.9	9		
394.7	5		
396.5	6		
<i>cis</i> IIb	0.0(29 037.1)	100	221
	1.7	136	239
	65.1	8	
	67.2	22	
	103.7	7	
	105.9	7	

58.8 cm<sup>-1</sup> above the electronic origin. The relative energies and intensities of these bands are similar to the corresponding bands of the all-*trans* compound. Both origins appear as doublets with splittings of  $\sim 2.1$  cm<sup>-1</sup>. Due to similarities of the electronic and vibronic origins with those of all-*trans*-nonatetraene, we assign these bands to the mono-*cis* nonatetraene (“*cis* I”) isomer indicated below.

*cis* I

A second set of *cis*-impurity bands is expressed as two nearly identical progressions. Relatively intense bands at  $-85.3$  and  $+87.1$  cm<sup>-1</sup> from the all-*trans*-isomer origin tentatively are assigned to the electronic origins of nonatetraenes with interior *cis* double bonds (*cis* IIa/*cis* IIb). Unlike the all-*trans*-isomer and *cis* isomer I, these two isomers do not exhibit strong vibronic origins. Bands that may correspond to the lowest frequency in-plane bending vibrations have relatively high frequencies (65 cm<sup>-1</sup>) and also may be due to methyl torsions. The intensity of the origins with respect to higher vibronic bands suggests that inversion symmetry, approximately valid for all-*trans*-nonatetraene and *cis*-isomer I, is destroyed in *cis*-isomers IIa and IIb. Further study of these and other *cis*-polyenes under isolated condi-

tions awaits the development of synthetic procedures that allow the preparation, purification, and identification of particular isomers.

#### IV. CONCLUSIONS

As discussed previously<sup>40</sup> and further established here, detailed analysis of the high resolution spectra and measurements of the fluorescence lifetimes of individual vibronic levels provide strong support for assigning the spectra presented in this paper to all-*trans* isomers. (1) The  $a_g$  vibrational frequencies in the one-photon spectra are identical to  $a_g$  frequencies that appear in the two-photon spectra. The  $S_1 \leftarrow S_0$  two-photon spectra are symmetry-allowed and should be dominated by the preponderant, all-*trans* species in these samples. (2) The fluorescent lifetimes for vibronic levels accessed in the one- and two-photon experiments ( $b_u$  and  $a_g$  symmetries, respectively) are comparable at low excess energies and essentially identical at higher excess energies ( $>1000$  cm<sup>-1</sup> for octatetraene,  $>400$  cm<sup>-1</sup> for nonatetraene) where intramolecular vibrational redistribution randomizes the excitation energy among modes of different symmetry. This “coalescing” of vibronic lifetimes also shows that the one-photon and two-photon spectra are due to the same species.

For nonatetraene the high intensity of bands built on vibronic origins indicates that even in polyenes without rigorous inversion symmetry, Herzberg–Teller vibronic coupling often is the dominant factor in determining the strength of  $S_0 \leftrightarrow S_1$  transitions. This conclusion is supported by the comparable fluorescence lifetimes of *cis* and *trans* octatetraenes in low temperature mixed crystals and explains why  $S_1 \leftarrow S_0$  transition strengths are remarkably similar for a wide range of *cis* and *trans* polyenes, with or without methyl groups, with or without solvent perturbations.

The  $S_1 \leftarrow S_0$  spectra of isolated, methyl-substituted tetraenes are complicated by the excitation of methyl torsions which in turn couple with low frequency, skeletal vibrations. The vibronic bands show characteristic splittings due to the tunneling of the methyl groups through low energy barriers in the  $S_1$  states. The spectrum of *trans,trans*-octatetraene is considerably simpler and offers an unprecedented view of the  $S_1$  vibronic levels of this prototypical polyene. Whereas methyl groups have a rather large influence on the free jet optical spectra, the  $S_1$  dynamics of the three tetraenes are remarkably similar. The fluorescence decay kinetics point to common nonradiative decay processes (attributed to *cis*–*trans* isomerization) with activation energies of  $\sim 2100$  cm<sup>-1</sup>. Differences between the decay rates of the  $2^1A_g$  states of the three polyenes can be explained by the significant contribution of methyl groups to the total density of vibronic states. The representative photochemistry of octatetraene and its considerably simpler  $2^1A_g \leftarrow 1^1A_g$  spectrum reinforce the choice of its *cis* and *trans* isomers as appropriate targets for understanding the excited state dynamics of isolated polyenes.

## ACKNOWLEDGMENTS

This work was supported by a Grant-in-Aid for Scientific Research on New Program (03NP0301) by the Department of Education, Science, and Culture of Japan. We also are grateful to the Royal Society/Japan Society for the Promotion of Science for support of A.J.B., and the Donors of the Petroleum Research Fund, administered by the American Chemical Society, a DuPont Fund grant to Bowdoin College, and the National Science Foundation U.S.–Japan Cooperative Photoconversion and Photosynthesis Research Program (Grant No. INT-9121965) for partial support of research by R.L.C. and B.A.T. We also acknowledge M. Aoyagi, I. Ohmine, D. W. Pratt, S. Saito, and M. Z. Zgierski for invaluable discussions on the electronic structure and dynamics of polyenes.

- <sup>1</sup>T. Yoshizawa and H. Kandori, in *Progress in Retinal Research*, edited by N. N. Osborne and G. J. Chader (Pergamon, Oxford, 1992), Vol. 11, pp. 33–55.
- <sup>2</sup>M. Mimuro and T. Katoh, *Pure Appl. Chem.* **63**, 123 (1991); R. R. Birge, *Biochim. Biophys. Acta* **1016**, 293 (1990).
- <sup>3</sup>R. J. Cogdell and H. A. Frank, *Biochim. Biophys. Acta* **895**, 63 (1987).
- <sup>4</sup>G. Feher and M. Y. Okamura, in *The Photosynthetic Bacteria*, edited by R. K. Clayton and W. R. Sistrom (Plenum, New York, 1978), pp. 349–386.
- <sup>5</sup>B. S. Hudson, B. E. Kohler, and K. Schulten, in *Excited States*, edited by E. C. Lim (Academic, New York, 1982), Vol. 6, p. 1.
- <sup>6</sup>B. E. Kohler, *Chem. Rev.* **93**, 41 (1993).
- <sup>7</sup>G. Orlandi, F. Zerbetto, and M. Z. Zgierski, *Chem. Rev.* **91**, 867 (1991).
- <sup>8</sup>B. S. Hudson and B. E. Kohler, *Chem. Phys. Lett.* **14**, 299 (1972); *J. Chem. Phys.* **59**, 4984 (1973).
- <sup>9</sup>K. Schulten and M. Karplus, *Chem. Phys. Lett.* **14**, 305 (1972).
- <sup>10</sup>K. Schulten, I. Ohmine, and M. Karplus, *J. Chem. Phys.* **64**, 4422 (1976); I. Ohmine, K. Schulten, and M. Karplus, *ibid.* **68**, 2348 (1978).
- <sup>11</sup>G. Herzberg and E. Teller, *Z. Phys. Chem. B* **21**, 410 (1933).
- <sup>12</sup>R. L. Christensen and B. E. Kohler, *J. Chem. Phys.* **63**, 1837 (1975).
- <sup>13</sup>V. Bonacic-Koutecky, M. Persico, D. Dohnert, and A. Sevin, *J. Am. Chem. Soc.* **104**, 6900 (1982).
- <sup>14</sup>G. J. M. Dormans, G. C. Groenenboom, and H. M. Buck, *J. Chem. Phys.* **86**, 4895 (1987).
- <sup>15</sup>F. Duschinsky, *Acta. Physiochim. URSS* **7**, 551 (1937).
- <sup>16</sup>F. Zerbetto, M. Z. Zgierski, F. Negri, and G. Orlandi, *J. Chem. Phys.* **89**, 3681 (1988).
- <sup>17</sup>M. Aoyagi, I. Ohmine, and B. E. Kohler, *J. Phys. Chem.* **94**, 3922 (1990).
- <sup>18</sup>I. Ohmine, *J. Chem. Phys.* **83**, 2348 (1985); U. Dinur and B. Scharf, *ibid.* **79**, 2600 (1983).
- <sup>19</sup>F. Zerbetto and M. Z. Zgierski, *J. Chem. Phys.* **93**, 1235 (1990).
- <sup>20</sup>H. Petek, A. J. Bell, R. L. Christensen, and K. Yoshihara, *J. Chem. Phys.* **96**, 2412 (1992).
- <sup>21</sup>B. E. Kohler and T. A. Spiglanin, *J. Chem. Phys.* **80**, 3091 (1984).
- <sup>22</sup>J. R. Ackerman, B. E. Kohler, D. Huppert, and P. M. Rentzepis, *J. Chem. Phys.* **77**, 3967 (1982).
- <sup>23</sup>B. E. Kohler, P. Mitra, and P. West, *J. Chem. Phys.* **85**, 4436 (1986); J. R. Ackerman and B. E. Kohler, *J. Am. Chem. Soc.* **106**, 3681 (1984); M. F. Granville, G. R. Holtom, and B. E. Kohler, *Proc. Nat. Acad. Sci. USA* **77**, 31 (1980); G. Adamson, G. Gradl, and B. E. Kohler, *J. Chem. Phys.* **90**, 3038 (1989).
- <sup>24</sup>M. F. Granville, G. R. Holtom, B. E. Kohler, R. L. Christensen, and K. L. D'Amico, *J. Chem. Phys.* **70**, 593 (1979); M. F. Granville, G. R. Holtom, and B. E. Kohler, *ibid.* **72**, 4671 (1980).
- <sup>25</sup>B. E. Kohler and P. West, *J. Chem. Phys.* **79**, 583 (1983).
- <sup>26</sup>R. L. Christensen and B. E. Kohler, *J. Phys. Chem.* **80**, 2197 (1976).
- <sup>27</sup>G. Gradl, B. E. Kohler, and C. Westerfield, *J. Chem. Phys.* **97**, 6064 (1992).
- <sup>28</sup>B. E. Kohler, *J. Lumin.* **60&61**, 458 (1994).
- <sup>29</sup>D. G. Leopold, V. Vaida, and M. F. Granville, *J. Chem. Phys.* **81**, 4210 (1984); V. Vaida, *Acc. Chem. Res.* **19**, 114 (1986).
- <sup>30</sup>L. A. Heimbrosk, J. E. Kenny, B. E. Kohler, and G. W. Scott, *J. Chem. Phys.* **75**, 4338 (1981).
- <sup>31</sup>R. M. Gavin, C. Weisman, J. K. McVey, and S. A. Rice, *J. Chem. Phys.* **68**, 522 (1978).
- <sup>32</sup>L. A. Heimbrosk, B. E. Kohler, and I. J. Levy, *J. Chem. Phys.* **81**, 1592 (1984).
- <sup>33</sup>W. J. Buma, B. E. Kohler, and K. Song, *J. Chem. Phys.* **92**, 4622 (1990); **94**, 6367 (1991).
- <sup>34</sup>W. J. Buma, B. E. Kohler, and K. Song, *J. Chem. Phys.* **94**, 4691 (1991).
- <sup>35</sup>W. J. Buma, B. E. Kohler, J. M. Nuss, T. A. Shaler, and K. Song, *J. Chem. Phys.* **96**, 4860 (1992).
- <sup>36</sup>W. G. Bouwman, A. C. Jones, D. Phillips, P. Thibodeau, C. Friel, and R. L. Christensen, *J. Chem. Phys.* **94**, 7429 (1990).
- <sup>37</sup>H. Petek, A. J. Bell, K. Yoshihara, and R. L. Christensen, *J. Chem. Phys.* **95**, 4739 (1991).
- <sup>38</sup>H. Petek, A. J. Bell, K. Yoshihara, and R. L. Christensen, *SPIE Proc.* **1638**, 345 (1992); H. Petek, A. J. Bell, H. Kandori, K. Yoshihara, and R. L. Christensen, in *Time Resolved Vibrational Spectroscopy V*, edited by H. Takahashi (Springer, Berlin, 1992), Vol. 5, pp. 198–199.
- <sup>39</sup>W. J. Buma, B. E. Kohler, and T. Shaler, *J. Chem. Phys.* **96**, 399 (1992).
- <sup>40</sup>H. Petek, A. J. Bell, Y. S. Choi, K. Yoshihara, B. A. Tounge, and R. L. Christensen, *J. Chem. Phys.* **98**, 3777 (1993).
- <sup>41</sup>W. H. Flygare, *Molecular Structure and Dynamics* (Prentice–Hall, Englewood Cliffs, 1978), pp. 128–135.
- <sup>42</sup>L. H. Spangler and D. W. Pratt, *J. Chem. Phys.* **84**, 4789 (1986).
- <sup>43</sup>D. R. Lide and D. Christensen, *J. Chem. Phys.* **35**, 1374 (1961).
- <sup>44</sup>A. E. Dorigo, D. W. Pratt, and K. N. Houk, *J. Am. Chem. Soc.* **109**, 6591 (1987).
- <sup>45</sup>P. J. Breen, J. A. Warren, E. R. Bernstein, and J. I. Seeman, *J. Chem. Phys.* **87**, 1917 (1987).
- <sup>46</sup>M. Ito, *J. Phys. Chem.* **91**, 517 (1987).
- <sup>47</sup>H. Longuet-Higgins, *Mol. Phys.* **6**, 445 (1963).
- <sup>48</sup>E. Hirota, *J. Chem. Phys.* **45**, 1984 (1966).
- <sup>49</sup>S. Saito and I. Ohmine (unpublished results).
- <sup>50</sup>X.-Q. Tan, D. J. Clouthier, R. H. Judge, D. F. Plusquellic, J. L. Tomer, and D. W. Pratt, *J. Chem. Phys.* **95**, 7862 (1991).
- <sup>51</sup>J. S. Horwitz, B. E. Kohler, and T. A. Spiglanin, *J. Chem. Phys.* **83**, 2186 (1985).
- <sup>52</sup>J. R. Ackerman and B. E. Kohler, *J. Chem. Phys.* **80**, 45 (1984).
- <sup>53</sup>J. R. Ackerman, S. A. Forman, M. Hossain, and B. E. Kohler, *J. Chem. Phys.* **80**, 39 (1984).
- <sup>54</sup>Y. S. Choi, T.-S. Kim, H. Petek, K. Yoshihara, and R. L. Christensen, *J. Chem. Phys.* **100**, 9269 (1994).